RSC Advances

ROYAL SOCIETY OF CHEMISTRY

www.rsc.org/advances

Thermal and pH Sensitive Multifunctional Polymer Nanoparticles for Cancer Imaging and Therapy

Tingjun Lei, PhD[1,2]; Romila Manchanda, PhD[1,3]; Alicia Fernandez-Fernandez, PhD[1,4]; Yen-Chih Huang, PhD[1]; Douglas Wright, BS[1], Anthony J McGoron, PhD[1,*]

[1] *Biomedical Engineering Department, Florida International University, 10555 West Flagler Street, Miami, FL 33174, USA*

[2] *Cirle, 1951 NW 7th Ave, Suite 13106, Miami, FL, 33136*

[3]*Department of Basic and Applied Sciences. Galgotias University, UP, 201308, India.*

[4]*Physical Therapy Department, Nova Southeastern University, 3200 S. University Dr., Fort Lauderdale, FL 33328, USA*

***Corresponding author:** Anthony J. McGoron., PhD.

Department of Biomedical Engineering, Florida International University,

10555 West Flagler Street, EC 2614, Miami, FL 33174, USA

E-mail: mcgorona@fiu.edu

Telephone: 305-348-1352

Fax: 305-348-6954

Word count for abstract: 142 words. Complete manuscript word count: 4950words.

Number of references: 48 references.

Number of figures: Six figures. Number of tables: Two tables.

Abstract

In this study, we prepared novel poly(Glycerol malate co-dodecanedioate) (PGMD) NPs containing an imaging/hyperthermia agent (IR820) and a chemotherapeutic agent (doxorubicin, DOX). The PGMD polymer was prepared by thermal condensation. IR820 and DOX loaded PGMD NPs were prepared using the single oil emulsion technique. The size of the NPs measured was around 150 nm. Drug loading efficiency of DOX and IR820 was around 4% and 8%, respectively. An acidic environment (pH=5.0) induced higher DOX release as compared to pH=7.4. DOX release was also enhanced by exposure to laser, which increased the temperature to 42°C. Cytotoxicity of the drug loaded NPs was comparable in MES-SA but was higher in Dx5 cells compared to free drug ($p<0.05$). The combination of hyperthermia and chemotherapy improved cytotoxicity in both cell lines. The NP formulation significantly improved the plasma half-life of IR820 in mice after tail vein injection.

Key words: poly(Glycerol malate co-dodecanedioate) (PGMD); hyperthermia; chemotherapy; IR820; multifunctional nanoparticles.

1. Introduction

Doxorubicin (DOX) and daunorubicin are examples of anthracycline antibiotics used in human cancer chemotherapy. Their use, like most anticancer drugs, has been limited by the fact that they are toxic to normal tissues and lack specificity to tumor sites [1]. Additionally, cancer cells can develop multidrug resistance (MDR) through the overexpression of P-glycoprotein (P-gp) reducing the retention of drugs, which further compromises the effect of these anthracycline drugs [2]. Several groups, including ours, have incorporated DOX into poly(lactic-co-glycolic acid) (PLGA) nanoparticles (NPs) to overcome MDR and achieve specific targeting to tumor cells [3-5].

Indocyanine green (ICG) is an FDA-approved near-infrared (NIR) dye studied intensively for its potential use in photodynamic therapy, photothermal therapy, and optical imaging [6-8]. Compared to visible light, absorption by human tissue is markedly reduced for NIR light, thus making it appropriate to be used for *in vivo* imaging. Our previous work investigated the commercially available cyanine dye IR820, which could be considered as an alternative to ICG because of similar optical and thermal properties [9]. Our study showed that IR820 is more stable than ICG in aqueous solution, with degradation half-times about double those of ICG. Although the ability of IR820 to produce heat after exposure to laser is somewhat less compared to ICG, the temperature increase obtained with the use of IR820 is still within the range needed for selective cancer cell hyperthermia (HT). We have been able to show that IR820 can be used in lieu of ICG in both optical imaging and hyperthermia applications [9].

Researchers have investigated "adjuvant" therapies which deliver heat and chemotherapeutic agents simultaneously to the tumor site, since it has been shown that combining chemotherapy and HT can result in better therapeutic outcomes compared to the use of chemotherapy alone [8,10]. Based on the promising results of "adjuvant" therapy, the development of multifunctional NPs as a delivery platform for drug and HT agents has become an emerging field in recent years. A commonly reported approach to combining chemotherapy and HT is by using iron oxide magnetic NPs to deliver drugs as well as to induce magnetic fluid HT [11,12]. Other approaches have focused on the incorporation of chemotherapeutic drug into polymeric NPs whose surface was coated with gold for HT delivery [13,14]. Our group has also reported the synthesis of multifunctional NPs with dual agent incorporation. We prepared PLGA NPs simultaneously loaded with DOX (anticancer agent) and ICG (optical/HT agent), and these particles resulted in increased cellular uptake and cytotoxicity in MDR cancer cell line Dx5 when compared to free DOX-ICG treatment [15]. The NPs, after exposure to laser, also resulted in better therapeutic outcomes than chemotherapy alone or HT alone in Dx5 cells [15]. In our most recent study, fast, short-term hyperthermia induced by optical dye NPs resulted in better therapeutic outcome than slow but longer-term hyperthermia, although a higher thermal dose is given in the case of long-term hyperthermia [16]. The cellular mechanisms demonstrating the benefits of laser induced NPs hyperthermia were also investigated [16].

However, DOX release from ICG-DOX-PLGA loaded NPs is very slow with approximately 50% still retained in the NPs after 30-day incubation in pH=7.4 phosphate buffered saline. The DOX release profile was not improved even after exposing the NPs to NIR laser, which elevated the temperature to ~43°C due to the presence of ICG. It seems that PLGA NPs are not sensitive to

external heat (~43°C) probably due to the high *Tg* (45°C-50°C) and high molecular weight (40,000-75,000 Da) of the PLGA used, which could have a large effect on the release rate [17]. Furthermore, the unmodified PLGA is hydrophobic, which typically only allows for encapsulation of hydrophobic drugs.

Several other polymers have been extensively investigated and used in pharmaceutical research based on their targeted drug delivery potential. Out of these polymer-based agents, polyester-based NPs in particular also have good shelf life, suitable physicochemical properties, and well-characterized degradation characteristics. However, their applications are potentially limited due to their inherent toxicity. Therefore, there is still a need to explore novel biodegradable polymers in order to overcome these disadvantages and to develop clinically translatable drug delivery vehicles.

In this study, we synthesized a novel polymer called poly(Glycerol malate co-dodecanedioate) (PGMD) through the thermal condensation method by mixing glycol, malic acid and 1,12-dodecanedioic acid (DDA). The formulation technique does not involve toxic chlorinated solvents, unlike the formulation of PLGA NPs, and the characteristics of PGMD NPs can be modified by modulating polymer composition, which provides versatility similar to that of PLGA. Specifically, the glass transition temperature (*Tg*) and hydrophilicity of PGMD NPs can be adjusted by changing the ratio of malic acid to DDA during the PGMD polymer synthesis process. These unique properties of PGMD polymer make it a good candidate for drug delivery applications. With the controllable *Tg*, we can easily manage the release profile, and the NPs can be used for incorporation of hydrophobic drugs or protein/DNA by adjusting their hydrophilicity.

In addition, PGMD has natural byproducts, such as glycol, malic acid and DDA, meaning that it is biocompatible and biodegradable. Following the synthesis of PGMD polymers, PGMD NPs were also successfully developed. The synthesis of PGMDNPs is easy and reproducible, and we can prepare uniform PGMDNPs for efficient drug delivery.

This paper focuses not only on the characterization of PGMD polymers and the synthesis of PGMD NPs, but also on exploring their potential for controlled release of drugs by different external stimuli. We performed *in vitro* cell drug uptake and toxicity testing of these NPs, as well as animal studies to investigate their *in vivo* biodistribution and pharmacokinetics. Thus, the rationale of this paper is to study and demonstrate the utility of these novel polymers for controlled release of loaded drugs and cancer imaging and therapy.

2. Results

2.1.Characterization of the polymer and NPs

Polymer characterization results are described in the supplementary materials. The size, zeta potential, polydispersity (PDI), and drug loading efficiency for void PGMD NPs, IR820-PGMD NPs and DOX-IR820-PGMD NPs are shown in Table 1. The size and shape of void PGMD NPs were also studied with scanning electron microscopy (SEM) (supplementary materials Figure S3). The size measurement results were confirmed with Dynamic Light Scattering (DLS) measurement (supplementary materials Figure S2). The difference between size measurements using SEM and DLS is probably due to DLS measuring the hydrodynamic radius, whereas SEM measures a dry sample. As a result, DLS measurements are typically larger than those obtained by SEM.

2.2.*In vitro* drug release

The release kinetics profile of DOX from DOX-IR820-PGMD NPs is shown in Figure 1. We observed a very slow release of DOX after the initial burst release from NPs in the absence of an external stimulus. However, either acidic buffer or heat can induce the release of DOX, indicating that PGMD NPs are thermal sensitive and pH sensitive. In pH 7.4 PBS, the release of DOX was around 49% in the first 5 hours, followed by a slow release reaching a total of only ~52% after 29 days. When these NPs are exposed to laser for 3 minutes in pH 7.4 PBS at the beginning of the experiment, 5 μM IR820 is able to increase the temperature to approximately 42°C, inducing a rapid release of ~81% DOX in 5 hours and 85% in 29 days. Additionally, an acidic environment (pH=5.0) can also induce the release of DOX from NPs up to ~72% in 5 hours and 86% in 29 days. DOX release was further enhanced when the NPs were placed in acidic buffer and exposed to laser for 3 minutes. Overall, ~90% DOX was released in 5 hours and ~95% in 29 days.

2.3. Subcellular localization

Subcellular localization images are shown in Figure 2. In Figure 2A, SKOV-3 lysosomes are stained with Lysotracker Blue, while Figure 2B shows the fluorescence of IR820 (red). Figure 2C, which is the merged image, shows that PGMD NPs mainly localized in the lysosomes as indicated by the overlap of the Lysotracker Blue and IR820. This means that PGMD NPs were probably taken up into cells by endocytosis.

As seen in Figure 3A, we observed that some DOX molecules were located in the nucleus. Since the free drug accumulates in the nucleus, we would expect the same fate for DOX leaked out from NPs [18]. On the other hand, DOX molecules that remained in the NPs stayed in the cytosol because size limitations prevent the NPs from crossing the nuclear pore complex. In Figure 3B, we can see that IR820 stayed in the cytosol for both the free form and when still encapsulated into NPs. Free form localization is due to the binding of free IR820 to cytoplasmic proteins such as ligandin [19]. In the merged picture shown in Figure 3C, the bright yellow dots in the cytosol indicate that the NPs are still in the process of releasing DOX and IR820.

2.4. Cellular uptake experiments

The cellular uptake results are consistent with the literature in that free DOX is taken up by cells mainly through diffusion [20], while the NP formulation is generally delivered into cells by endocytosis [21]. An improved DOX cellular uptake profile by NPs was observed as compared to their free form in the MDR cell line Dx5 as shown in Figure 4, probably due to reduced elimination of drug with NP delivery since the NP formulation can overcome the P-gp effect. However, NPs did not result in greater DOX uptake in drug-sensitive cancer cell line MES-SA compared to the free drug form, because these cells do not have mechanisms to affect drug retention.

2.5. *In vitro* cytotoxicity

MES-SA and Dx5 cell proliferation following IR820-PGMD NPs, DOX-IR820-PGMD NPs and free DOX and IR820 incubation w/ or w/o laser exposure is shown in Figure 5. A solution of 0.05 mg/ml IR820-PGMD NPs or DOX-IR820-PGMD NPs (containing approximately 5 μM

IR820) can increase the temperature from 37 °C to 42 °C following exposure to an 808 nm NIR laser (power density is 1440 J/cm^2) for 3 minutes. Based on this finding, we used a concentration of 0.05 mg/mL IR820-PGMD NPs and DOX-IR820-PGMD NPs in our hyperthermia study and compared them to free DOX-IR820 treatment. Interestingly, we found that MES-SA cell growth was inhibited starting at 5 μM IR820 concentrations, which is likely due to the fact that MES-SA cells are more sensitive to environmental stressors than Dx5. The same phenomenon was observed in MES-SA cells incubated with 5 μM free IR820 in our previous study [9]. IR820-PGMD NPs significantly killed cancer cells after laser exposure compared to the no-laser NP treated group in both cell lines due to the HT effect. It is important to note that laser treatment by itself did not have an effect on cell growth.

Our results showed that, although DOX-IR820-PGMD NPs seem to have higher cytotoxicity as compared to DOX-IR820 in MES-SA cells without laser exposure, the difference did not reach statistical significance. Accordingly, the difference in cancer cell killing effect is not statistically significant when comparing the NPs to their free form after laser exposure in MES-SA. On the other hand, DOX-IR820-PGMD NPs show much higher cytotoxicity than free DOX-IR820 treatment in Dx5, and the difference is statistically significant ($p<0.05$).

Additionally, the combination of HT and chemotherapy caused enhanced cancer cell killing in both cell lines compared to either chemotherapy or HT alone ($p<0.05$). Based on our results, the treatment of Dx5 cells with NPs containing 4 μM DOX and 3 minutes of laser exposure can improve the cytotoxicity and the cell killing effect to reach levels comparable to those observed in DOX-sensitive MES-SA cells.

2.6. *In vivo* studies

The pharmacokinetics study of IR820 concentration in plasma at different time points after injection is shown in a semi-log scale in Figure 6A. The quantitative dye content analysis showed that IR820 was present in plasma in significantly higher amounts for NP formulation compared to free IR820 24 hours after injection ($p<0.05$). The monoexponential calculated plasma half-lives for free IR820, IR820-PGMDNPs, and DOX-IR820-PGMDNPs were approximately 14.5 min, 18.7 min, and 19.5 min respectively, based on an average initial injected IR820 plasma concentration of 4μg/mL. It is not possible to differentiate, at the time of measurement, drug that had been released from the NPs from drug that remains encapsulated in the NPs. Following injection, the in vivo behavior of IR820 released from NPs and free IR820 will be the same, and so it is not surprising that the plasma concentrations of drug from the two groups (free and encapsulated in NPs) were similar at early time points. This is most likely due to the initial fast release of IR820 from the NPs in the first hours (Supplementary Materials Figure S4), which results in a rapid decrease of IR820 plasma concentration after injection of the NPs formulation. After initial distribution, the plasma elimination of IR820 from the NPs becomes slower compared to the elimination of free IR820, probably due to the slow and sustained release of IR820 from the NPs (Supplementary Materials Figure S4). This phenomenon indicates that the IR820 encapsulated inside the NPs is protected by the NPs, and thus has a slower elimination rate as compared to free IR820. That is, after injection of the NPs formulation, only IR820 that has been released from the NPs is eliminated, whereas entrapped IR820 is protected from elimination. This results in a prolonged circulation time.

The DOX plasma concentration was measured at different time points, as shown in Figure 6B. Based on the loading efficiency of DOX in DOX-IR820-PGMD NPs, and an IR820 dose of 0.24 mg/kg, the average initial concentration of injected DOX in plasma was approximately 2 μg/mL. The calculated plasma half-lives in the two-compartment model were approximately 36 min (distribution half-life) and 22 hours (elimination half-life).

Our organ studies showed that IR820, both when in free form and encapsulated into NPs, is processed primarily by hepatobiliary excretion and starts to accumulate in the liver within 5-10 minutes after injection. However, organs such as the kidney and the lungs also have considerable contents of IR820 after 24 hours, indicating uptake by the reticuloendothelial system. The DOX-IR820-PGMD NP group demonstrated significantly lower dye content in the kidneys compared to the free dye group ($p=0.04$), and 2.6 times smaller dye content in the liver, although the latter did not reach statistical significance ($p=0.08$). As for the IR820-PGMD NPs, dye content was lower in kidneys and lungs, but the differences also did not reach statistical significance. The lack of statistical significance is probably due to the small number of subjects used in the study as well as individual variability. DOX organ content after 24 hours injection was not detectable in any tissue samples; that is, the DOX fluorescence intensity was not greater than the background autofluorescence, probably due to the sub-therapeutic DOX dose used in this study. Based on these results, we can say that DOX-IR820-PGMD NPs demonstrate decreased renal clearance, and probably slower liver clearance, compared to free dye.

3. Discussion

The MW of PGMD polymer is around 3000 Da, which is consistent with the literature stating that polycondensation of monomers would preferentially yield low MW polymers [22]. When high MW polymers are desired, ring opening polymerization is preferred [23]. Jesus et al. have reported the synthesis of a polyester dendritic scaffold based on the monomer unit (2,2-bis(hydroxymethyl)propanoic acid) with a measured polymer MW around 4000 Da [24]. The PGMD NPs we obtained are in the 100-150 nm range, which can potentially avoid premature clearance by the reticuloendothelial system. The negative charge on the nanoparticle surface may be due to the presence of carboxylic groups from malic acid and DDA, and the hydrolysis of the ester groups [25]. The addition of pluronic F127 as surfactant on the particle surface can possibly increase the distance between the particle surface and the shear surface [26], which could result in a decrease of the zeta potential. Similarly, Huang et al. reported that negatively charged paclitaxel-loaded poly(*n*-butyl cyanoacrylate) nanoparticles were synthesized and the increase of pluronic F127 can lead to lower zeta potential [27].

Loading of IR820 and DOX into the PGMD NPs increased the PDI of the NPs as compared to void NPs. Cheng et al. reported that increased PDI was observed with increasing loading amount of docetaxel into PLGA–PEG (polyethylene glycol) NPs [28]. The observed increase in DOX-IR820-PGMD NP zeta potential after addition of DOX and IR820 as compared to void PGMD NPs may be caused by a zeta potential change towards neutral due to incorporated DOX amino groups.

The release of DOX from PGMD NPs was increased after exposure to laser. This is perhaps because of the phase change of the PGMD polymer (Tg=42.2°C) at high temperatures, which

increases the release of DOX from the polymer matrix. There are several synthetic polymers reported to be sensitive to temperature change, such as acrylamide-based hydrogels, especially poly[N-isopropylacrylamide] (PNIPA) hydrogel, and elastin-like polypeptides [29-31]. Zhang et al. reported that a synthetic PNIPA hydrogel released 20-30% more of its 5-fluorouracil load at 37°C compared to 10°C [32]. In addition, an acidic environment can also induce higher DOX release, probably due to the accelerated hydrolysis, which resulted in faster degradation of the PGMD polymer [33].

It is well documented that tumor sites have lower pH than blood and healthy tissue [34,35]. Therefore, a rapid release of DOX from PGMD NPs in an acidic environment could be beneficial in cancer therapy. Moreover, the heating of IR820 by an external NIR laser can further induce release of DOX at tumor site. Generally, DOX release from the PGMD NPs was faster in the first phase as compared to our previous study of DOX release from PLGA NPs [15], which is probably due to the fact that PGMD has a much lower molecular weight compared to the PLGA used in that study (3 kDa v.s. 75 kDa). Zolnik reported that polymer MW is a key factor in determining release rate, and slow release was observed in high MW polymers (70 kDa) [17]. On the other hand, PGMD is more hydrophilic than PLGA due to the addition of malic acid in the polycondensation process. Thus, when using these two polymers to synthesize NPs, PLGA is estimated to have a stronger hydrophobic-hydrophobic interaction with DOX than is PGMD, which could be another reason that a higher amount of DOX was released from PGMD NPs compared to PLGA NPs for the same time period.

In the subcellular localization study, DOX fluorescence was detected in both the cytosol and the nucleus. We have demonstrated that the fate of PGMD NPs is mainly localizing in lysosomes. Some of the NPs are able to escape endo-lysosomal degradation and release their payload in the cytosol. The escape process primarily takes place through selective reversal of the NPs' surface charge (from anionic to cationic) in the acidic endo-lysosomal compartment, causing the NPs to interact with the endo-lysosomal compartment membrane and to escape into the cytosol [36].

The NPs result in significant higher cell killing than the free form of DOX and IR820 in Dx5, but not in MES-SA. This is because MES-SA is a sensitive cell line and does not overexpress P-gp, so the NPs do not have advantages in increasing cellular uptake over the free form of DOX and IR820. All these results are in accordance with the cellular uptake study, in which we observed comparable cellular uptake of DOX-IR820 and DOX-IR820-PGMD NPs in MES-SA cells, whereas the NPs result in much higher uptake of DOX in Dx5 cells compared to when the DOX was in free drug. Our previous study of DOX-PLGA NPs had shown that NPs can overcome the P-gp pump efflux effect and increase the uptake and cytotoxicity of DOX in MDR cell lines, because the NP formulation can protect the DOX drug from being recognized by the P-gp pump [37]. Our result also showed that the NPs kill more Dx5 cells after exposure to laser as compared to when the drugs are in their free form ($p<0.05$). Improved cancer cell killing can be achieved with a combination of HT and chemotherapy. Our previous study demonstrated that mild cell apoptosis can be induced by mild HT [38]. Furthermore, the therapeutic effect of DOX can be potentially augmented because mild HT can enhance cell membrane permeability and fluidity, and in turn result in accumulation of drug inside cancer cells, especially for MDR cancer cells.

The increased IR820 plasma half-life and prolonged circulation time in NP formulation may present an advantage over the free form by stabilizing the dye and allowing longer image collection periods in imaging studies. Additionally, a widened therapeutic window may be available when providing HT as an adjuvant therapy, thanks to prolonged exposure of tissues to IR820. DOX plasma half-life is also enhanced when they are encapsulated in NPs. This is a significant improvement over literature reports for free DOX which described a distribution half-life of ~2 minutes and elimination half-life of ~10.3 hours in mice [39]. Other researchers have also observed prolonged DOX plasma half-lives in different animal models when a nanoformulation, such as liposomes or NPs, was used [40-42]. For instance, Reddy et al. reported that DOX loaded poly(butyl cyanoacrylate) NPs prolonged DOX half-life ~1.5 fold as compared to free DOX in rats [43]. Based on available literature reports nanoformulations seem to result in improved pharmacokinetic profiles, in many cases as a result of their size and surface properties, ability to stabilize encapsulated drugs, and reduced liver metabolism and renal clearance [44,45]. This could impact the therapeutic efficacy of these agents because higher overall exposure and prolonged exposure profiles can result in enhanced *in vivo* tumor uptake and improved therapeutic efficacy. Additionally, circulation time could be further increased after NP pegylation [46-48]. Although having such long-circulating agents may be a concern in terms of potential toxicity effects, most of the NPs are expected to be cleared from the animals by 24 hours, so that the chances to induce NP toxicity via accumulation in the liver is negligible, based on our estimation (supplementary materials Table S4).

4. Methods

4.1. Drugs and chemicals

Malic acid, 1, 12-Dodecanedioic acid (DDA), dimethylsulfoxide (DMSO>99.9%, reagent grade), pluronic F-127, micro bicinchonic acid (BCA) protein assay kits, Dulbecco phosphate-buffered saline (DPBS), phosphate buffered saline (PBS), IR820, penicillin–streptomycin solution, tetrahydrofuran (THF) and trypsin-EDTA were purchased from Sigma-Aldrich (St. Louis, Missouri). Doxorubicin hydrochloride (DOX-HCl; MW 579.95) was purchased from Waterstone Technology (Waterstone Technology, CA). Glycerol was purchased from MP Biomedical (Solon OH).

4.2. Synthesis and characterization of PGMD polymer

PGMD polymers were prepared following Mingueo's paper with the modification of adding malic acid [49]. Briefly, glycerol and a combination of DDA and malic acid in 1:1 molar ratio were mixed and heated up to 120°C for 48 hours. The molar ratio of DDA to malic acid was 7:3. Methods for characterization of the polymer are provided in the supplementary materials.

4.3. Synthesis of NPs

DOX-IR820-PGMD NPs and IR820-PGMD NPs were synthesized using the oil-in-water emulsification solvent evaporation method. The detailed synthesis procedures are described in supplementary materials.

4.4. Characterization of NPs

The size of void PGMD NPs, IR820-PGMD NPs and DOX-IR820-PGMD NPs was measured by dynamic light scattering (DLS) using a Malvern Zetasizer (Malvern Instruments, Worcestershire, United Kingdom). Size measurements were taken at 25°C using a 1:30 (vol/vol) dilution of the

NP suspension in distilled water. Zeta potential of the NPs dispersed in deionized (DI) water was measured by the same Zetasizer.

4.5. Drug loading

The NPs were dissolved in DMSO (1 mL), and the absorption spectrum of the samples was evaluated using a Cary WinUV spectrophotometer (Varian/Agilent Technologies, Switzerland).

4.6.*In Vitro* studies of NPs

Human uterine sarcoma MES-SA cells, and their MDR counterpart (P-gp overexpressing derivative MES-SA/Dx5 (Dx5)) cells, human ovarian carcinoma cancer cells (SKOV-3), McCoy's 5A medium, and fetal bovine serum were purchased from American Type Culture Collection (Manassas, VA). Formalin, 24-well tissue culture plates, and d-poly coverslips were purchased from Fisher Scientific (Pittsburg, PA). Penicillin was purchased from Sigma-Aldrich. All the cells were cultured in McCoy's 5A medium supplemented with 1% penicillin and 10% fetal bovine serum, and kept in a 37°C cell incubator with a humidified atmosphere of 5% CO_2 and 95% air.

4.6.1. *In vitro* drug release kinetics profile in DOX-IR820-PGMD NPs

Briefly, 5 mg of DOX-IR820-PGMD NPs were resuspended in 3 mL of 0.01 M PBS (pH=7.4 or pH=5.0). Next, the sample was divided equally into three Eppendorf tubes, which were shaken at 35 rpm at 37°C in an incubator. The tubes were then removed from the incubator every hour up to the first 5 hours, and then after 24 hours. Each time, the samples were centrifuged at 14,000 rpm for 30 minutes. Following this, the supernatant was collected in 4.5-mL cuvettes, and the

DOX and IR820 content were estimated using a spectrofluorometer (Jobin Yvon Horiba, Edison, NJ). The NPs were again suspended in fresh PBS solution and incubated for subsequent time release measurements. This process was repeated at regular time intervals, every 7 days after the first day, and the release study was done for a period of 29 days.

The release of DOX from DOX-IR820-PGMD NPs after exposure to laser in different pH was also studied. Briefly, the NPs were measured and resuspended in 3 mL PBS with different pH (pH=7.4 or pH=5.0) to obtain 5 μM IR820. Then, the suspension was exposed to an 808-nm NIR laser (RLDH808-1200-5, Roithner Laserthchnik, Austria) for 3 minutes with power density of 1440 J/cm^2. Finally, the suspension was centrifuged and processed as previously described.

4.6.2. Subcellular localization of the NPs

To study the intracellular localization of IR820-PGMD NPs and DOX-IR820-PGMD NPs, SKOV-3 cells were seeded in a 24-well tissue culture plate, and incubated overnight to reach confluence. On the second day, cell medium was removed and then replaced with 0.5 mL of 0.05 mg/ml IR820-PGMD NPs (5 μM IR820) and 0.05 mg/ml DOX-IR820-PGMD NPs (4 μM DOX plus 5 μM IR820). The plates were kept in an incubator for 24 hours and protected from light exposure. After incubation, cells were washed with PBS three times and fixed with 4% (vol/vol) formaldehyde. Then, the specimens were observed by fluorescence microscopy (Olympus IX81, Japan) with a 20X objective or 60X water merged objective. The fluorescence was imaged at λex (490 nm), λem (580 nm) for DOX, λex (775 nm), λem (845 nm) for IR820, and λex (355 nm), λem (420 nm) for LysoTracker Blue (Invitrogen, NY). A CCD camera was used to capture the signals and the images were software-merged with pseudo color (IPLab, Qimaging, Canada).

Subcellular localization of the IR820-PGMD NPs was identified by incubating 5 μM Lysotracker Blue with cells for 10 min at the end of the experiment.

4.6.3. Cellular uptake studies

Two cell lines (MES-SA and Dx5) were used to study the cellular uptake of unencapsulated DOX and IR820 (designated as free DOX + IR820) and to compare with the uptake of the NP formulation. Detailed methods are provided in the supplementary materials.

4.6.4. Cytotoxicity assessment

Cell viability was measured with the sulforhodamine B (SRB) assay (Invitrogen, NY) after 24 hours. In this study, the cytotoxicities of seven different treatments (free DOX plus IR820, IR820-PGMD NPs, DOX-IR820-PGMD NPs, free DOX plus IR820 w/ laser, IR820-PGMD NPs w/ laser, DOX-IR820-PGMD NPs w/ laser, and laser only) were investigated. In the laser only group the cells were exposed to laser for 3 minutes with no NPs, drug or dye added. The detailed procedure for laser and drug exposure is described in a prior publication [8]. We also tested the cytotoxicity of void PGMD NPs at higher concentrations (0.1 mg/mL) than those used in the experiment (supplementary materials Figure S5). An average (± SD) "cell growth" from three experiments was plotted. Cell growth values were generated by normalizing the data from each treatment to the control values which did not receive any treatments.

4.7. *In vivo* pharmacokinetic study and biodistribution study

Nd4 Swiss Webster mice (25–30 grams, 9 weeks old) were purchased from Harlan (Indianapolis, IN), kept under standard housing conditions, and fed ad libitum. All protocols followed the

regulations of the Institutional Animal Care and Use Committee. Mice were randomly assigned to different experimental groups based on different time points, namely 15 minutes, 30 minutes, 60 minutes, and 24 hours. On the day of the experiment, the animals were anesthetized with pentobarbital and injected i.v. through the tail vein with a solution of NPs in PBS. The concentration of injected NPs [50] and an injection volume of 0.2 mL. At the terminal time point for all groups (15min, 30min, 60min, and 24h), plasma samples were collected in order to study the pharmacokinetic profiles of IR820 and DOX. Plasma samples were obtained by heart puncture followed by centrifugation for 3 minutes at 12,000 rpm. Then, the plasma was collected and centrifuged again for 3 minutes at 12,000 rpm to ensure separation of any remaining blood cells. Lastly, plasma was removed incubated in DMSO (1:50 volume ratio plasma: DMSO) for thirty minutes and centrifuged at 6,000 rpm for 15min. IR820 and DOX content in the supernatant was measured with a spectrofluorometer at 785 nm and 482 nm excitation respectively, using previously created calibration curves of IR820 and DOX in DMSO. The time profile of IR820 plasma concentration was fitted to a monoexponential decay model using Matlab (MathWorks, Massachusetts), whereas the time profile of DOX plasma concentration was fitted to a biexponential decay model. The choice of model was determined by the best R^2 fit value. In addition to plasma measurements, in the 24h group the IR820 in liver, lungs, kidneys, and intestines were also extracted at the terminal time point. The quantitative measurements of IR820 content in different organs after 24h were performed by dye extraction in DMSO following the procedure described by Saxena et al. for ICG [51].

4.8. Statistical significance

Statistical significance was identified by ANOVA or t-test (SPSS, Chicago, Illinois) for the difference among treatment groups and control groups. A p-value < 0.05 was considered to be statistically significant.

5. Conclusions

The novelty of this study is the synthesis of a thermal and pH sensitive polymer which provides a tunable and predictable pharmacokinetic release profile using thermal or pH stimuli. This novel and adjustable PGMD NP delivery vehicle was loaded with the chemotherapy agent DOX and the imaging and HT agent IR820. The resulting NP formulations can be used to improve cellular uptake and cytotoxicity in the MDR cancer cell line Dx5. The combination of chemotherapy and HT also enhanced DOX cytotoxicity in both MES-SA and Dx5 compared to single therapy alone, indicating that less DOX can be used when hyperthermia "adjuvant" cancer therapy is introduced. *In vivo* studies showed that the IR820 in this NP formulation has a longer plasma half-life than free IR820, providing longer imaging collection times for cancer diagnostics, and potentially widening the window for HT applications. An increase in DOX plasma half-life was also observed in NP formulation, which results in an increased exposure of tumor cells to the chemotherapeutic drug; coupled with the passive targeting provided by the enhanced permeability and retention (EPR) effect may increase tumor uptake [52]. This could potentially lead to improvements in therapeutic efficacy, and there is the potential to further expand the effect via formulation modifications which could include active targeting. Thus, DOX-IR820-PGMD NPs have promising applications as theranostic agents with multifunctional imaging, HT and chemotherapy capabilities.

Acknowledgements

We thank the Biomedical Engineering Department at Florida International University (FIU) for allowing the use of their facilities, AMERI at FIU for providing the SEM images, and NIH for providing partial funding from grant 1R15CA167571-01A1.

References

[1] Chari, R. V. J. Targeted delivery of chemotherapeutics: tumor-activated prodrug therapy. *Advanced Drug Delivery Reviews.* **1998**, *31*, 89-104.

[2] Yi, C.; Gratzl, M. Continuous in Situ Electrochemical Monitoring of Doxorubicin Efflux from Sensitive and Drug-Resistant Cancer Cells. *Biophysical Journal.* **1998**, *75*, 2255-2261.

[3] Yoo, H. S.; Oh, J. E.; Lee, K. H.; Park, T. G. Biodegradable nanoparticles containing doxorubicin-PLGA conjugate for sustained release. *Pharmaceutical Research.* **1999**, *16*, 1114-1118.

[4] Yoo, H. S.; Park, T. G. Biodegradable polymeric micelles composed of doxorubicin conjugated PLGA–PEG block copolymer. *Journal of Controlled Release.* **2001**, *70*, 63-70.

[5] Lee, E. S.; Na, K.; Bae, Y. H. Doxorubicin loaded pH-sensitive polymeric micelles for reversal of resistant MCF-7 tumor. *Journal of Controlled Release.* **2005**, *103*, 405-418.

[6] Abels, C.; Fickweiler, S.; Weiderer, P.; Bäumler, W.; Hofstädter, F.; Landthaler, M.; Szeimies, R. M. Indocyanine green (ICG) and laser irradiation induce photooxidation. *Archives of Dermatological Research.* **2000**, *292*, 404-411.

[7] Dorshow, R. B.; Bugaj, J. E.; Burleigh, B. D.; Duncan, J. R.; Johnson, M. A.; Jones, W. B. Noninvasive Fluorescence Detection of Hepatic and Renal Function. *Journal of Biomedical Optics.* **1998**, *3*, 340-345.

[8] Tang, Y.; McGoron, A. J. Combined effects of laser-ICG photothermotherapy and doxorubicin chemotherapy on ovarian cancer cells. *Journal of Photochemistry and Photobiology B: Biology.* **2009**, *97*, 138-144.

[9] Fernandez-Fernandez, A.; Manchanda, R.; Lei, T.; Carvajal, D. A.; Tang, Y.; Kazmi, S. Z.; McGoron, A. J. Comparative study of the optical and heat generation properties of IR820 and indocyanine green. *Mol Imaging.* **2012**, *11*, 99-113.

[10] Overgaard, J. Combined adriamycin and hyperthermia treatment of a murine mammary carcinoma in vivo. *Cancer Research.* **1976**, *36*, 3077-3081.

[11] Jordan, A.; Scholz, R.; Maier-Hauff, K.; Johannsen, M.; Wust, P.; Nadobny, J.; Schirra, H.; Schmidt, H.; Deger, S.; Loening, S.; Lanksch, W.; Felix, R. Presentation of a new magnetic field therapy system for the treatment of human solid tumors with magnetic fluid hyperthermia. *Journal of Magnetism and Magnetic Materials.* **2001**, *225*, 118-126.

[12] Pankhurst, Q. A.; Connolly, J.; Jones, S. K.; Dobson, J. Applications of magnetic nanoparticles in biomedicine. *J Phys D Appl Phys.* **2003**, *36*, R167-R181.
[13] Park, H.; Yang, J.; Lee, J.; Haam, S.; Choi, I.-H.; Yoo, K.-H. Multifunctional Nanoparticles for Combined Doxorubicin and Photothermal Treatments. *ACS Nano.* **2009**, *3*, 2919-2926.
[14] Cheng, F. Y.; Su, C. H.; Wu, P. C.; Yeh, C. S. Multifunctional polymeric nanoparticles for combined chemotherapeutic and near-infrared photothermal cancer therapy in vitro and in vivo. *Chem Commun.* **2010**, *46*, 3167-3169.
[15] Tang, Y.; Lei, T.; Manchanda, R.; Nagesetti, A.; Fernandez-Fernandez, A.; Srinivasan, S.; McGoron, A. J. Simultaneous delivery of chemotherapeutic and thermal-optical agents to cancer cells by a polymeric (PLGA) nanocarrier: an in vitro study. *Pharmaceutical Research.* **2010**, *27*, 2242-2253.
[16] Lei, T.; Fernandez-Fernandez, A.; Manchanda, R.; Huang, Y.-C.; McGoron, A. J. Near-infrared dye loaded polymeric nanoparticles for cancer imaging and therapy and cellular response after laser-induced heating. *Beilstein Journal of Nanotechnology.* **2014**, *5*, 313-322.
[17] Zolnik, B. S.; Leary, P. E.; Burgess, D. J. Elevated temperature accelerated release testing of PLGA microspheres. *Journal of Controlled Release.* **2006**, *112*, 293-300.
[18] Gieseler, F.; Biersack, H.; Brieden, T.; Manderscheid, J.; Nüßler, V. Cytotoxicity of anthracyclines: Correlation with cellular uptake, intracellular distribution and DNA binding. *Annals of Hematology.* **1994**, *69*, S13-S17.
[19] Kaplowitz, N.; Kuhlenkamp, J.; Clifton, G. Hepatic glutathione S-transferases: identification by gel filtration and in vitro inhibition by organic anions. *Proceedings of the Society for Experimental Biology and Medicine.* **1975**, *149*, 234-237.
[20] Misra, R.; Sahoo, S. K. Intracellular trafficking of nuclear localization signal conjugated nanoparticles for cancer therapy. *European Journal of Pharmaceutical Sciences.* **2010**, *39*, 152-163.
[21] Qaddoumi, M. G.; Gukasyan, H. J.; Davda, J.; Labhasetwar, V.; Kim, K. J.; Lee, V. H. Clathrin and caveolin-1 expression in primary pigmented rabbit conjunctival epithelial cells: role in PLGA nanoparticle endocytosis. *Molecular Vision.* **2003**, *9*, 559-568.
[22] Vroman, I.; Tighzert, L. Biodegradable Polymers. *Materials.* **2009**, *2*, 307-344.
[23] Löfgren, A.; Albertsson, A.-C.; Dubois, P.; Jérôme, R. Recent Advances in Ring-Opening Polymerization of Lactones and Related Compounds. *Journal of Macromolecular Science, Part C.* **1995**, *35*, 379-418.
[24] Padilla De Jesús, O. L.; Ihre, H. R.; Gagne, L.; Fréchet, J. M. J.; Szoka, F. C. Polyester Dendritic Systems for Drug Delivery Applications: In Vitro and In Vivo Evaluation. *Bioconjugate Chemistry.* **2002**, *13*, 453-461.
[25] Müller, R. H.; Lherm, C.; Herbort, J.; Blunk, T.; Couvreur, P. Alkylcyanoacrylate drug carriers: I. Physicochemical characterization of nanoparticles with different alkyl chain length. *International Journal of Pharmaceutics.* **1992**, *84*, 1-11.
[26] Duro, R.; Gómez-Amoza, J. L.; Martínez-Pacheco, R.; Souto, C.; Concheiro, A. Adsorption of polysorbate 80 on pyrantel pamoate: effects on suspension stability. *International Journal of Pharmaceutics.* **1998**, *165*, 211-216.
[27] Huang, C.-Y.; Chen, C.-M.; Lee, Y.-D. Synthesis of high loading and encapsulation efficient paclitaxel-loaded poly(n-butyl cyanoacrylate) nanoparticles via miniemulsion. *International Journal of Pharmaceutics.* **2007**, *338*, 267-275.

[28] Cheng, J.; Teply, B. A.; Sherifi, I.; Sung, J.; Luther, G.; Gu, F. X.; Levy-Nissenbaum, E.; Radovic-Moreno, A. F.; Langer, R.; Farokhzad, O. C. Formulation of functionalized PLGA–PEG nanoparticles for in vivo targeted drug delivery. *Biomaterials.* **2007**, *28*, 869-876.

[29] Chilkoti, A.; Dreher, M. R.; Meyer, D. E.; Raucher, D. Targeted drug delivery by thermally responsive polymers. *Advanced Drug Delivery Reviews.* **2002**, *54*, 613-630.

[30] Bikram, M.; West, J. L. Thermo-responsive systems for controlled drug delivery. *Expert Opinion on Drug Delivery.* **2008**, *5*, 1077-1091.

[31] Meyer, D. E.; Shin, B. C.; Kong, G. A.; Dewhirst, M. W.; Chilkoti, A. Drug targeting using thermally responsive polymers and local hyperthermia. *Journal of Controlled Release.* **2001**, *74*, 213-224.

[32] Zhang, X.-Z.; Zhuo, R.-X.; Cui, J.-Z.; Zhang, J.-T. A novel thermo-responsive drug delivery system with positive controlled release. *International Journal of Pharmaceutics.* **2002**, *235*, 43-50.

[33] Gillies, E. R.; Fréchet, J. M. J. pH-Responsive Copolymer Assemblies for Controlled Release of Doxorubicin. *Bioconjugate Chemistry.* **2005**, *16*, 361-368.

[34] Vaupel, P.; Kallinowski, F.; Okunieff, P. Blood-Flow, Oxygen and Nutrient Supply, and Metabolic Microenvironment of Human-Tumors - a Review. *Cancer Research.* **1989**, *49*, 6449-6465.

[35] Engin, K.; Leeper, D. B.; Cater, J. R.; Thistlethwaite, A. J.; Tupchong, L.; Mcfarlane, J. D. Extracellular Ph Distribution in Human Tumors. *Int J Hyperther.* **1995**, *11*, 211-216.

[36] Panyam, J.; Zhou, W. Z.; Prabha, S.; Sahoo, S. K.; Labhasetwar, V. Rapid endo-lysosomal escape of poly(DL-lactide-co-glycolide) nanoparticles: implications for drug and gene delivery. *FASEB Journal.* **2002**, *16*, 1217-1226.

[37] Lei, T. J.; Srinivasan, S.; Tang, Y.; Manchanda, R.; Nagesetti, A.; Fernandez-Fernandez, A.; McGoron, A. J. Comparing cellular uptake and cytotoxicity of targeted drug carriers in cancer cell lines with different drug resistance mechanisms. *Nanomed-Nanotechnol.* **2011**, *7*, 324-332.

[38] Tang, Y.; McGoron, A. J. Increasing the rate of heating: a potential therapeutic approach for achieving synergistic tumour killing in combined hyperthermia and chemotherapy. *Int J Hyperthermia.* **2013**, *29*, 145-155.

[39] Gustafson, D. L.; Rastatter, J. C.; Colombo, T.; Long, M. E. Doxorubicin pharmacokinetics: Macromolecule binding, metabolism, and excretion in the context of a physiologic model. *Journal of Pharmaceutical Sciences.* **2002**, *91*, 1488-1501.

[40] Gulyaev, A. E.; Gelperina, S. E.; Skidan, I. N.; Antropov, A. S.; Kivman, G. Y.; Kreuter, J. Significant Transport of Doxorubicin into the Brain with Polysorbate 80-Coated Nanoparticles. *Pharmaceutical Research.* **1999**, *16*, 1564-1569.

[41] Rahman, A.; Carmichael, D.; Harris, M.; Roh, J. K. Comparative pharmacokinetics of free doxorubicin and doxorubicin entrapped in cardiolipin liposomes. *Cancer Research.* **1986**, *46*, 2295-2299.

[42] Gabizon, A. A.; Barenholz, Y.; Bialer, M. Prolongation of the Circulation Time of Doxorubicin Encapsulated in Liposomes Containing a Polyethylene Glycol-Derivatized Phospholipid: Pharmacokinetic Studies in Rodents and Dogs. *Pharmaceutical Research.* **1993**, *10*, 703-708.

[43] Reddy, L. H.; Murthy, R. S. Pharmacokinetics and biodistribution studies of Doxorubicin loaded poly(butyl cyanoacrylate) nanoparticles synthesized by two different techniques. *Biomed Pap Med Fac Univ Palacky Olomouc Czech Repub.* **2004**, *148*, 161-166.
[44] Li, S. D.; Huang, L. Pharmacokinetics and biodistribution of nanoparticles. *Mol Pharmaceut.* **2008**, *5*, 496-504.
[45] Moghimi, S. M.; Hunter, A. C.; Andresen, T. L. Factors Controlling Nanoparticle Pharmacokinetics: An Integrated Analysis and Perspective. *Annu Rev Pharmacol.* **2012**, *52*, 481-503.
[46] Panagi, Z.; Beletsi, A.; Evangelatos, G.; Livaniou, E.; Ithakissios, D. S.; Avgoustakis, K. Effect of dose on the biodistribution and pharmacokinetics of PLGA and PLGA–mPEG nanoparticles. *International Journal of Pharmaceutics.* **2001**, *221*, 143-152.
[47] Gref, R.; Lück, M.; Quellec, P.; Marchand, M.; Dellacherie, E.; Harnisch, S.; Blunk, T.; Müller, R. H. 'Stealth' corona-core nanoparticles surface modified by polyethylene glycol (PEG): influences of the corona (PEG chain length and surface density) and of the core composition on phagocytic uptake and plasma protein adsorption. *Colloids and Surfaces B: Biointerfaces.* **2000**, *18*, 301-313.
[48] Zahr, A. S.; Davis, C. A.; Pishko, M. V. Macrophage Uptake of Core−Shell Nanoparticles Surface Modified with Poly(ethylene glycol). *Langmuir.* **2006**, *22*, 8178-8185.
[49] Migneco, F.; Huang, Y.-C.; Birla, R. K.; Hollister, S. J. Poly(glycerol-dodecanoate), a biodegradable polyester for medical devices and tissue engineering scaffolds. *Biomaterials.* **2009**, *30*, 6479-6484.
[50] Maarek, J.-M. I.; Holschneider, D. P.; Harimoto, J. Fluorescence of indocyanine green in blood: intensity dependence on concentration and stabilization with sodium polyaspartate. *Journal of Photochemistry and Photobiology B: Biology.* **2001**, *65*, 157-164.
[51] Saxena, V.; Sadoqi, M.; Shao, J. Polymeric nanoparticulate delivery system for Indocyanine green: Biodistribution in healthy mice. *International Journal of Pharmaceutics.* **2006**, *308*, 200-204.
[52] Maeda, H.; Wu, J.; Sawa, T.; Matsumura, Y.; Hori, K. Tumor vascular permeability and the EPR effect in macromolecular therapeutics: a review. *Journal of Controlled Release.* **2000**, *65*, 271-284.

Tables and Figure Captions

Table 1. Mean size, PDI, zeta potential of PGMD NPs measured using DLS; and percent loading efficiencies measured using a spectrophotometer (n = 8).

Figure 1. Cumulative percent release of DOX from DOX-IR820-PGMD NPs under different experimental conditions.

Figure 2. Subcellular localization of IR820-PGMD NPs in SKOV-3. All the images were taken after 24 hours incubation of NPs with cells and were merged with pseudo color by software (IPLab, Qimaging). A. Lysotracker Blue fluorescence; B. IR820 fluorescence of IR820-PGMD NPs; C. merged picture of A and B; D. phase contrast image. Scale bar represents 20 μm.

Figure 3. Subcellular localization of DOX-IR820-PGMD NPs in SKOV-3 cells after 24h incubation. All the images were merged with pseudo color by software (IPLab, Qimaging). A. DOX fluorescence of DOX-IR820-PGMD NPs; B. IR820 fluorescence of DOX-IR820-PGMD NPs; C. merged picture of A and B; D. phase contrast image. The concentrations of IR820 and DOX were kept at 5 μM and 4 μM, respectively. Scale bar represents 20 μm.

Figure 4. 24-hour intracellular DOX uptake in MES-SA and Dx5 cells; n=3 experiments, 3 wells per treatment. * $P<0.05$ (by t-test) between NP formulation and their free form for each cell line, indicating significant differences due to loading of DOX into PGMD NPs.

Figure 5. 24-hour cytotoxicity profile of NPs and their free form w/ or w/o 3 minutes laser exposure in MES-SA and Dx5 cells; n=3, 4 wells/treatment. * $P<0.05$ (by ANOVA) indicates significant differences in cytotoxicity between free form and NP groups in Dx5 due to the bypassing of P-gp; ** $P<0.05$ (by ANOVA) indicates significant differences in cytotoxicity between laser-treated and non-treated groups due to HT enhancement of cancer cell killing.

Figure 6. A. IR820 plasma concentration at different time points after i.v. injection in free IR820 or NP treatment. The data were expressed in a semi-log scale. B. DOX plasma concentration at different time points after i.v. injection in DOX-IR820-PGMD NP treatment.

Table 2. Quantitative IR820 organ content 24 hours after i.v. injection of IR820-PGMD NPs, IR820 or DOX-IR820-PGMD NPs. Values represent average±SD. * $P<0.05$, significant difference between free IR820 and NP dye content in kidneys and plasma.

Table 1:

Formulation	Size (nm)	Polydispersity	Zeta potential (mV)	IR820 loading (w/w %)	DOX loading (w/w %)
PGMD void NPs	92± 19.6	0.095±0.015	-34.3±1.6	N/A	N/A
IR820-PGMD NPs	109±8.2	0.151±0.006	-29.1±7.5	8.4±0.5	N/A
DOX-IR820-PGMDNPs	125±19.7	0.182±0.023	-20.3±2.9	8.1±0.6	4.3±0.3

Figure 1:

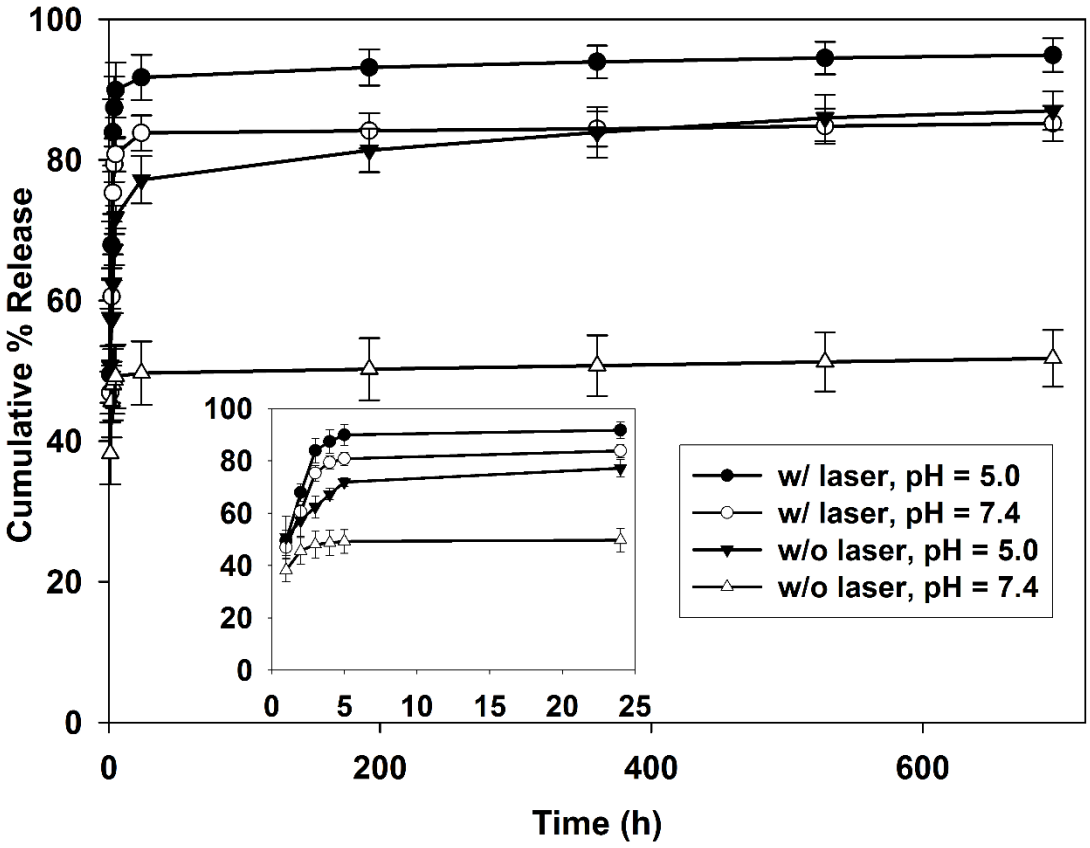

Figure 2:

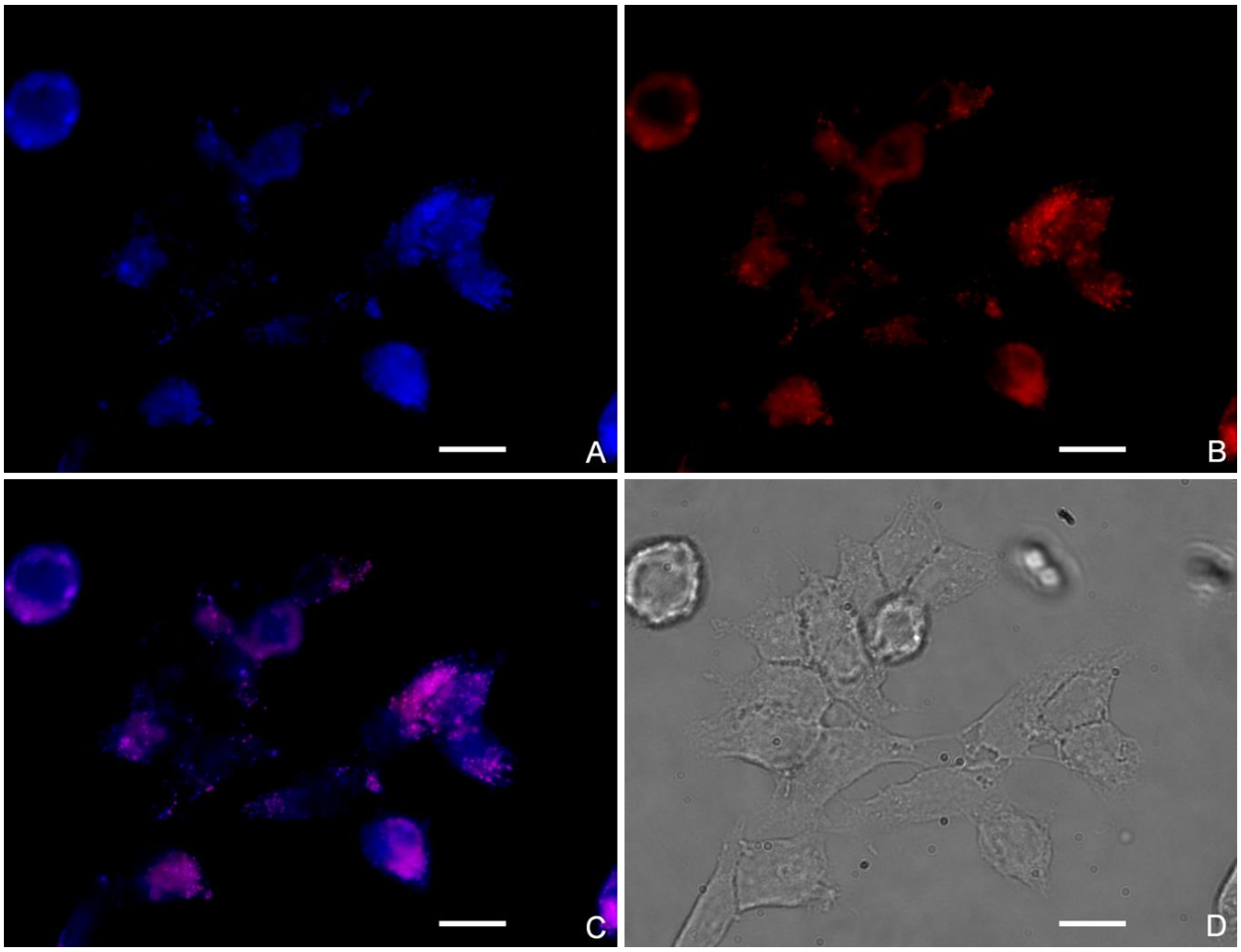

Figure 3:

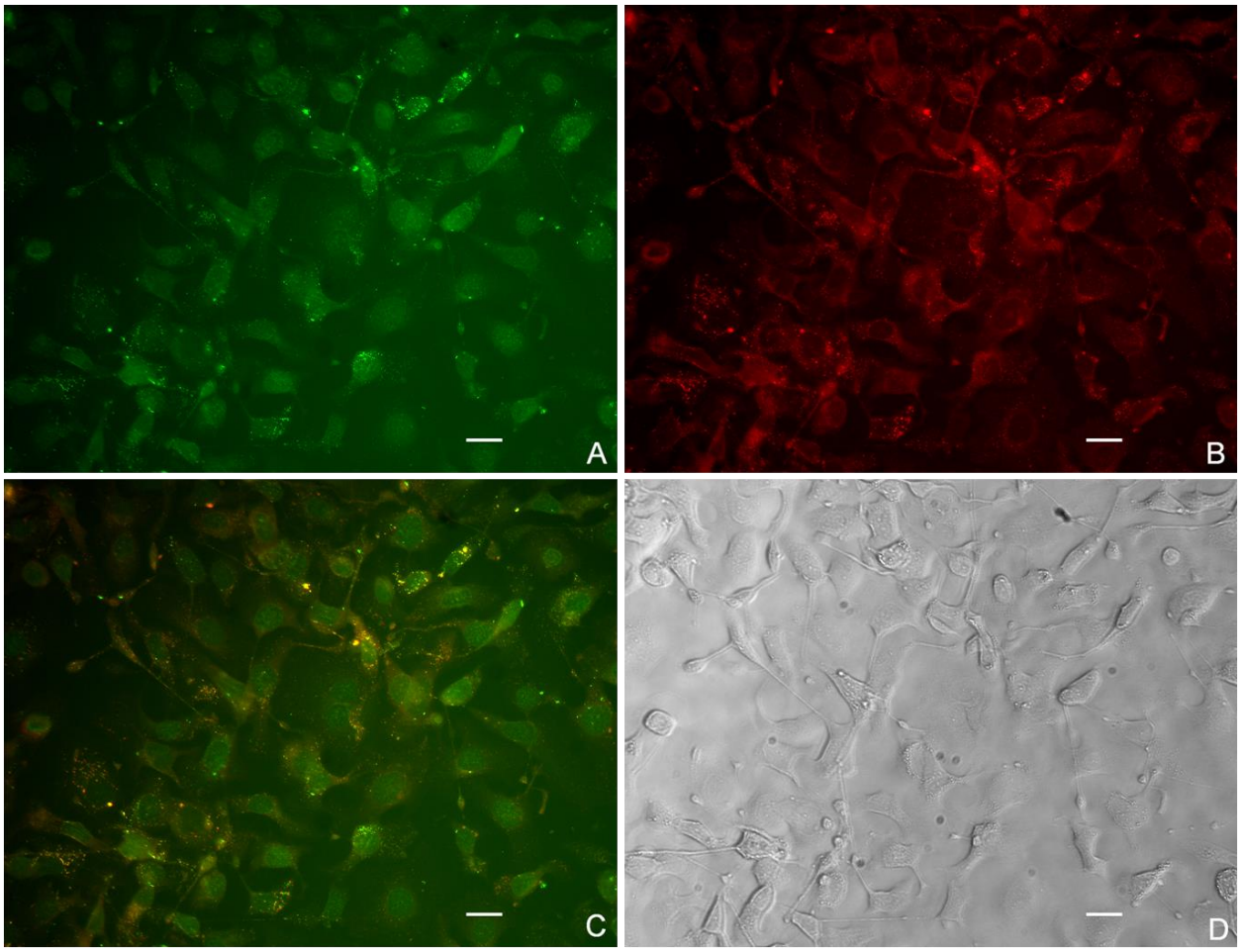

Figure 4:

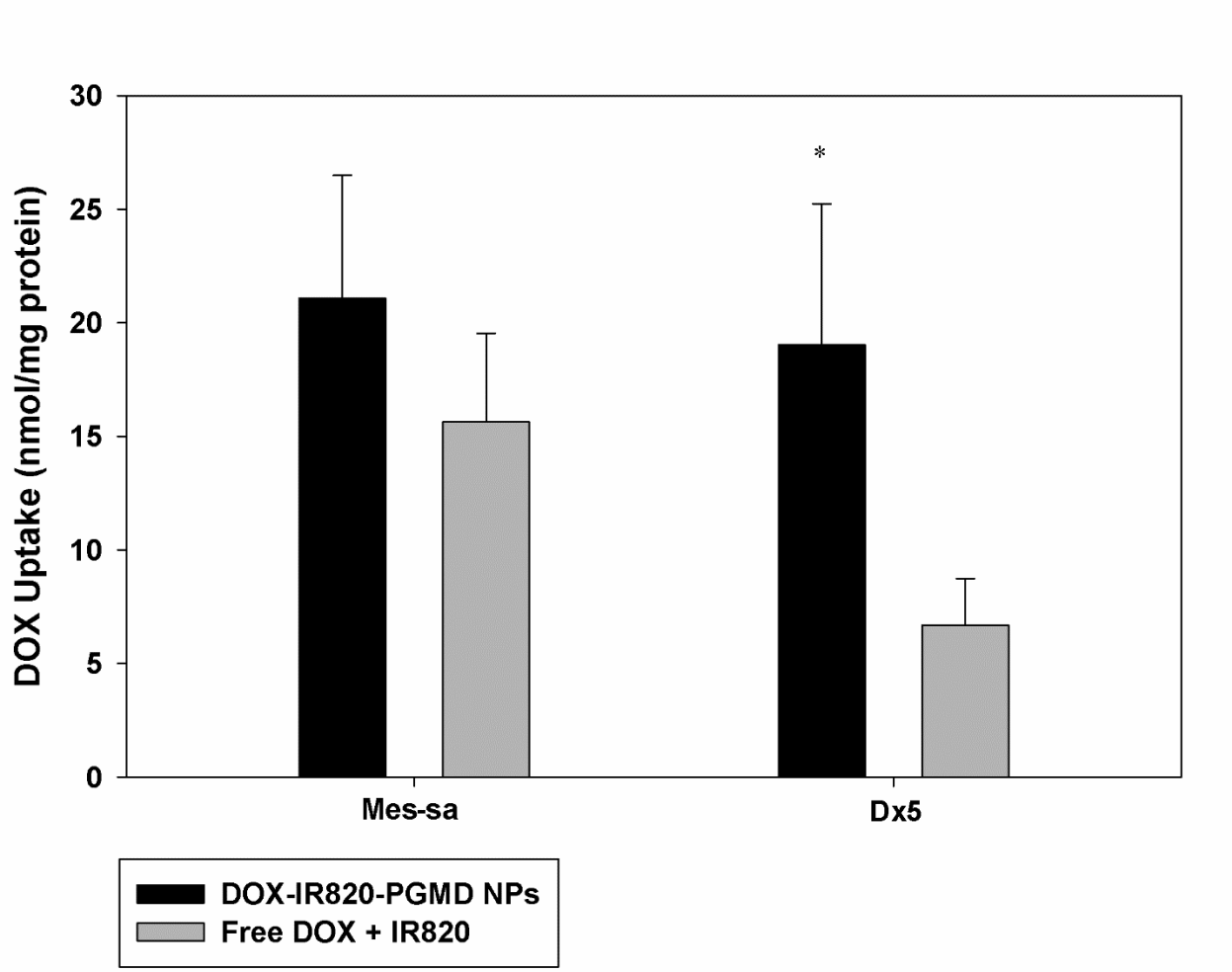

Figure 5:

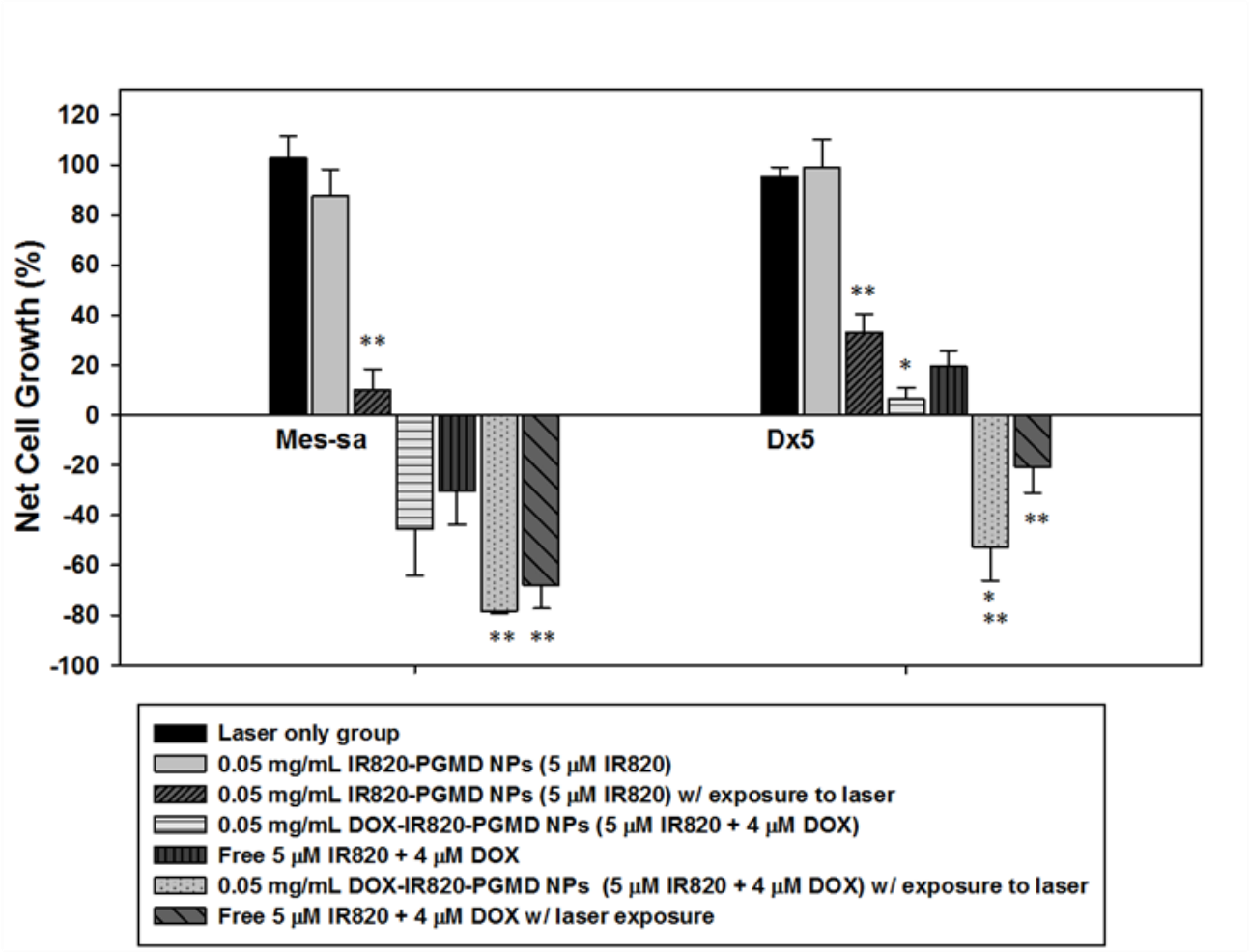

Figure 6:

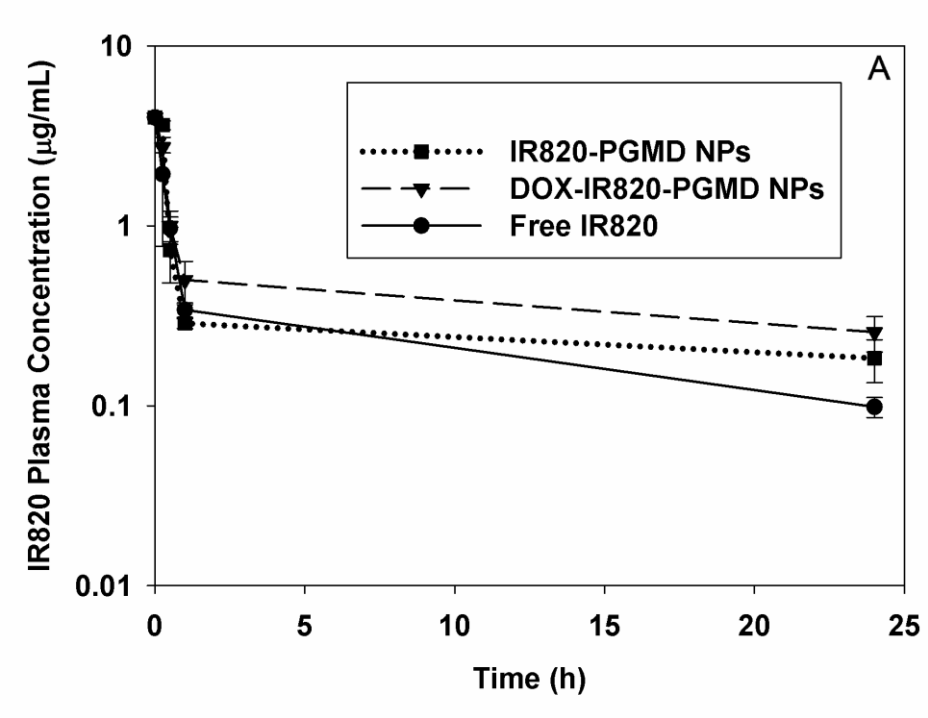

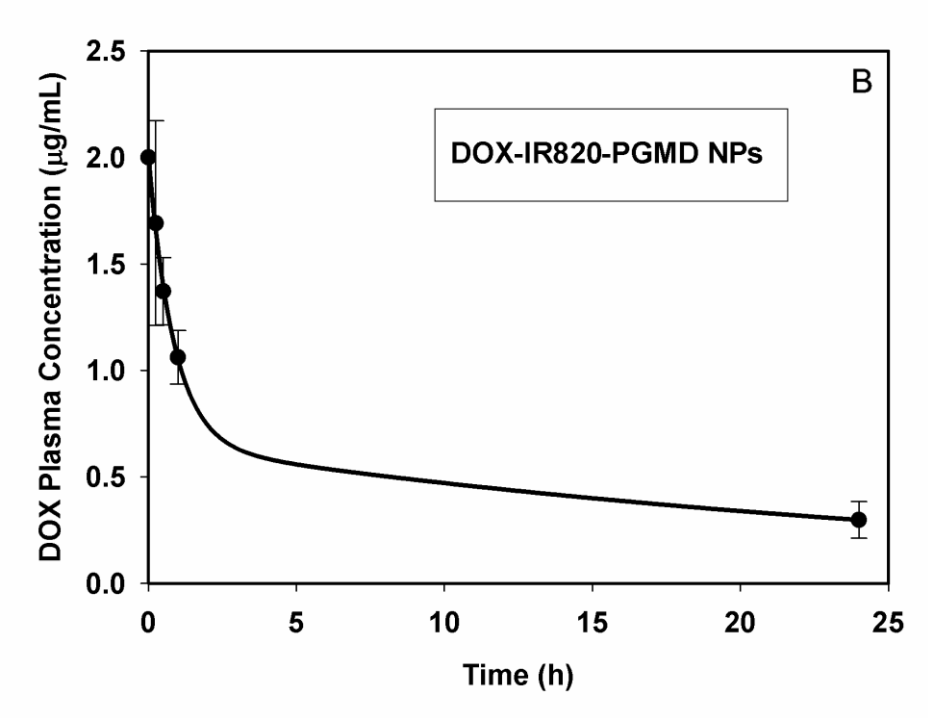

1 Table 2:

24h organ and plasma IR820 dye content (n=3)	Liver (μg/g)	Lungs (μg/g)	Intestines (μg/g)	Kidneys (μg/g)	Plasma (μg/mL)
IR820-PGMD NPs	0.21±0.09	0.23±0.07	0.07±0.02	0.25±0.09	*0.18±0.04
IR820	0.21±0.11	0.28±0.03	0.05±0.006	0.41±0.11	0.10±0.003
DOX-IR820-PGMD NPs	0.08±0.01	0.26±0.08	0.05±0.02	*0.21±0.04	*0.26±0.06

2

3